Supplementary materials for

Segmentation and radial anisotropy of the deep crustal magmatic system beneath the Cascades arc

Chengxin Jiang[1], Brandon Schmandt[2], Geoffrey A. Abers[3], Eric Kiser[4], Meghan S. Miller[1]

1. Research School of Earth Sciences, The Australian National University, Acton, ACT, Australia

2. Department of Earth and Planetary Sciences, University of New Mexico, Albuquerque, NM, USA

3. Department of Earth and Atmospheric Sciences, Cornell University, Ithaca, NY, USA

4. Department of Geosciences, University of Arizona, Tucson, AZ, USA

Content:

Text S1. *A summary of prior controlled source P-velocity studies in the western Cascades.*

- Tréhu et al., [*1994*] conducted a N-S controlled-source survey along the forearc just outside the western edge of the focus area for this study. They estimated that the North American crust extends to ~40 km depth (their Figure 2) where it may be underlain by the subducting Juan de Fuca slab's basaltic crust followed by the oceanic Moho. In this location the largest velocity contrast may be the Juan de Fuca Moho rather than the base of the North America crust. As the slab deepens to the east in our focus area, we expect an increasing mantle wedge between the base of the North American crust and the Juan de Fuca slab.
- Miller et al., [*1997*] conducted a N-S controlled source P velocity survey and estimated ~48 km thick crust beneath the western Cascades near the latitude of Mount St. Helens. However, the deepest Moho estimated in that study was outside of the area sampled by PmP (dashed lines in their Plate 2) and primarily inferred from forward modeling of Pn arrivals and gravity, which may have different structural sensitivity. Additionally, Miller et al., [*1997*] noted that the crust-mantle boundary may be "extremely transitional" (page 8 of that paper) and that the uppermost mantle is very slow, ~7.6 km/s P velocity.
- Parsons et al., [*1998*] conducted a W-E controlled source P velocity survey that intersected the southern end of the Miller et al., [*1997*] transect between Mt. St. Helens and Mt. Rainier. Parsons et al., [*1998*] came to different interpretations where the lines intersect. They interpreted ~35-40 km crust thickness beneath the western Cascades (their Figure 2B). Similar to Miller et al., [*1997*], Parsons et al., [*1998*] indicated a transitional crust-mantle boundary and slow, ~7.8 km/s P-velocity, uppermost mantle.
- Brocher et al., [*2003*] synthesized results from several controlled source surveys along the Cascades margin and showed a pattern of strong reflectivity of the Juan de Fuca Moho near the coast and strong continental PmP beneath the axis of the Cascades arc and farther inboard, with often weak or absent PmP beneath the intervening forearc and the western Cascades. They interpreted the variably weak PmP in the forearc as a consequence of uppermost mantle wedge serpentinization consistent with slow Pn velocities of ~7.6-7.8 km/s mentioned in the studies above.
- Kiser et al., [*2016*] conducted controlled source P-velocity surveys with dense NW-SE and SW-NE transects centered on Mt. St. Helens (their Figure 2). Their results indicated ~35-40 km thick crust across much of the focus area for this study (Figure 1a black box).

Text S2. *A justification on the use of the Moho reference model of Schmandt et al., [2015].*

In this surface wave study, we are not trying to determine if one of the above high-frequency P-wave models of the Moho is more correct than the others as this level of detail has little influence on our Rayleigh and Love wave dispersion measurements.

We suggest that a Moho model rooted in sensitivity to S-velocity changes with depth is appropriate for a tomography model using Rayleigh and Love wave dispersion measurements that are dominantly sensitive to S-velocity [e.g., *Julià et al., 2000*]. Teleseismic Ps receiver functions are dominantly sensitive to S-velocity contrasts and use lower frequencies than controlled source P-wave reflection and refraction studies. Therefore, surface waves and receiver functions would sense the crust-mantle boundary in a more similar way than surface waves and high-frequency P-wave reflection/refraction. We note that we allow the Moho to move +/- 5 km from the reference model so we are not directly assuming the reference model.

Multiple controlled source P-wave studies [*Parsons et al., 1998; Kiser et al., 2016*] and teleseismic Ps receiver function studies are consistent with our chosen reference model with a +/- 5 km prior distribution for the McMC inversion [*Shen and Ritzwoller, 2016; Ma and Lowry, 2017; Mann et al., 2020*]. While not all studies agree in detail, we think it is reasonable to apply Moho constraints, such as those from Schmandt et al., [*2015*], that are rooted in lower frequency measurements with dominant sensitivity to S-wave velocity contrasts because we are conducting low frequency S-velocity tomography. In addition, we found the shallow Moho in our study region is also observed in crustal models constrained from other geophysical data, such as Pn tomography [*Buehler & Shearer, 2016*] and joint inversion of receiver function and gravity [*Ma & Lowry, 2017*].

The absolute S-velocities and Moho depths from our model are in good agreement with other recent models that jointly inverted receiver functions and surface wave dispersion data to obtain absolute velocities [e.g., *Shen and Ritzwoller, 2016*]. The Moho reference model from Schmandt et al., [*2015*] also iteratively inverted receiver functions in multiple frequency bands, Rayleigh wave dispersion, and Rayleigh wave ellipticity measurements. So, while the model does not have the detail of controlled source surveys it does not conflict with existing constraints on absolute S-velocities in the region. Additionally, the lower crust velocities we find near Mt. St. Helens, S-velocities of ~3.7-4.0 km/s, are plausible when compared to the nearby controlled source P-velocity estimates of ~7.0-7.5 km/s [*Miller et al., 1997; Parsons et al., 1998; Kiser et al., 2016*]. Together they imply Vp/Vs values of ~1.75-2, which are common for lower crustal lithologies [*Hacker et al., 2015*].

Table S1. *A list of the seismic networks used in this study along with their associated DOIs.*

Seismic network	**Citation**
XD	Ken Creager. (2014). *Collaborative Research: Illuminating the architecture of the greater Mount St. Helens magmatic systems from slab to surface* [Data set]. International Federation of Digital Seismograph Networks. https://doi.org/10.7914/SN/XD_2014
XU	Steve Malone, Ken Creager, Stephane Rondenay, Tim Melbourne, & Geoffrey Abers. (2006). *Collaborative Research: Earthscope integrated investigations of Cascadia subduction zone tremor, structure and process* [Data set]. International Federation of Digital Seismograph Networks. https://doi.org/10.7914/SN/XU_2006
YW	Mike Brudzinski, & Richard Allen. (2007). *Resolving structural control of episodic tremor and slip along the length of Cascadia* [Data set]. International Federation of Digital Seismograph Networks. https://doi.org/10.7914/SN/YW_2007
XC	David James, & Matthew Fouch. (2006). *Collaborative Research: Understanding the causes of continental intraplate tectonomagmatism: A case study in the Pacific Northwest* [Data set]. International Federation of Digital Seismograph Networks. https://doi.org/10.7914/SN/XC_2006
XQ	Alan Levander. (2007). *Seismic and Geodetic Investigations of Mendocino Triple Junction Dynamics* [Data set]. International Federation of Digital Seismograph Networks. https://doi.org/10.7914/SN/XQ_2007
TA	IRIS Transportable Array. (2003). *USArray Transportable Array* [Data set]. International Federation of Digital Seismograph Networks. https://doi.org/10.7914/SN/TA
US (permanent)	Albuquerque Seismological Laboratory (ASL)/USGS. (1990). *United States National Seismic Network* [Data set]. International Federation of Digital Seismograph Networks. https://doi.org/10.7914/SN/US
UW (permanent)	University of Washington. (1963). *Pacific Northwest Seismic Network - University of Washington* [Data set]. International Federation of Digital Seismograph Networks. https://doi.org/10.7914/SN/UW
ZG	Gene Humphreys. (2006). *Origin of the Columbia River Basalts and Uplift of the Wallowa Mountains* [Data set]. International Federation of Digital Seismograph Networks. https://doi.org/10.7914/SN/ZG_2006

Table S2. *Model space for each model variable used in this study.*

Model variable	**Model space**
1st B-spline coefficients of crust for modeling Vs and Aniso	2.0-3.8 km/s, -15% – 15%
2nd B-spline coefficients of crust for modeling Vs and Aniso	2.5-4.0 km/s, -15% – 15%
3rd B-spline coefficients of crust for modeling Vs and Aniso	2.5-4.0 km/s, -15% – 15%
4th B-spline coefficients of crust for modeling Vs and Aniso	2.8-4.0 km/s, -15% – 15%
5th B-spline coefficients of crust for modeling Vs and Aniso	3.0-4.2 km/s, -15% – 15%
Moho depth	±5 km relative to the local values of the reference model of Schmandt et al., (2015)
Vs and Aniso for the single mantle layer	3.9-4.8 km/s, , -15% – 15%

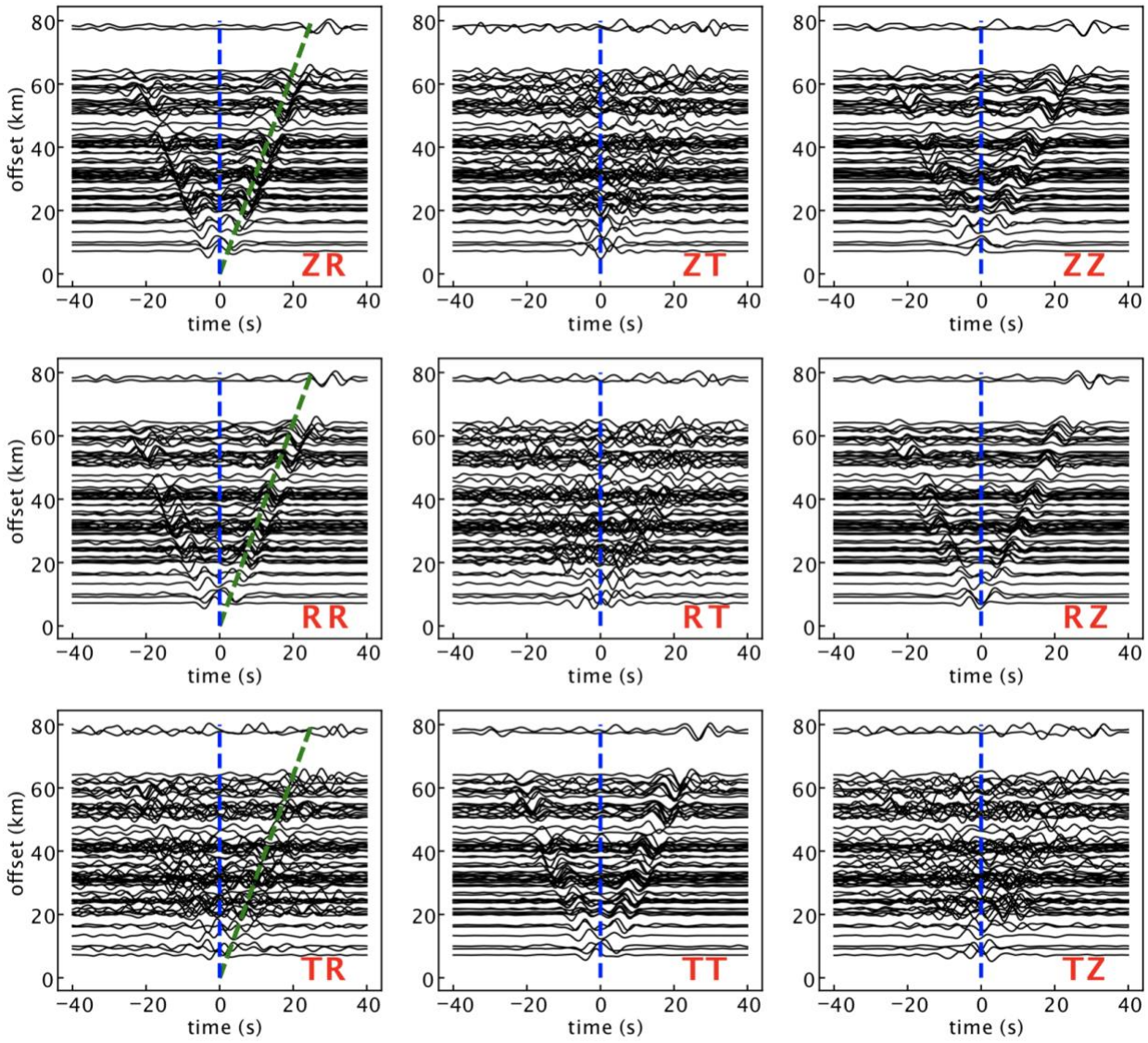

Figure S1. Same as Figure 2, but for the 9-component cross-correlation tensors. Note the energy on the cross-component between the vertical and tangent is much weaker compared to the others.

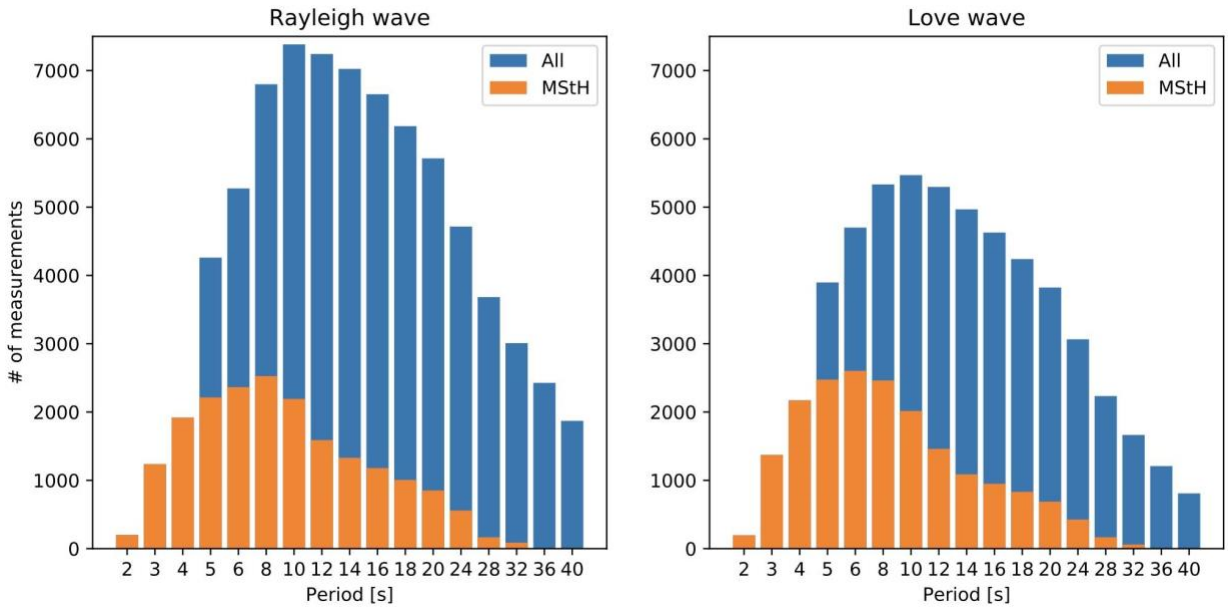

Figure S2. The number of dispersion measurements used in the tomography at different periods for both Rayleigh and Love wave. The orange bars show the statistics based upon the stations located in the black box of Figure 1, while the blue bars use all stations across the broad region. Note that the period increments along the x-axis of the figure are not uniform.

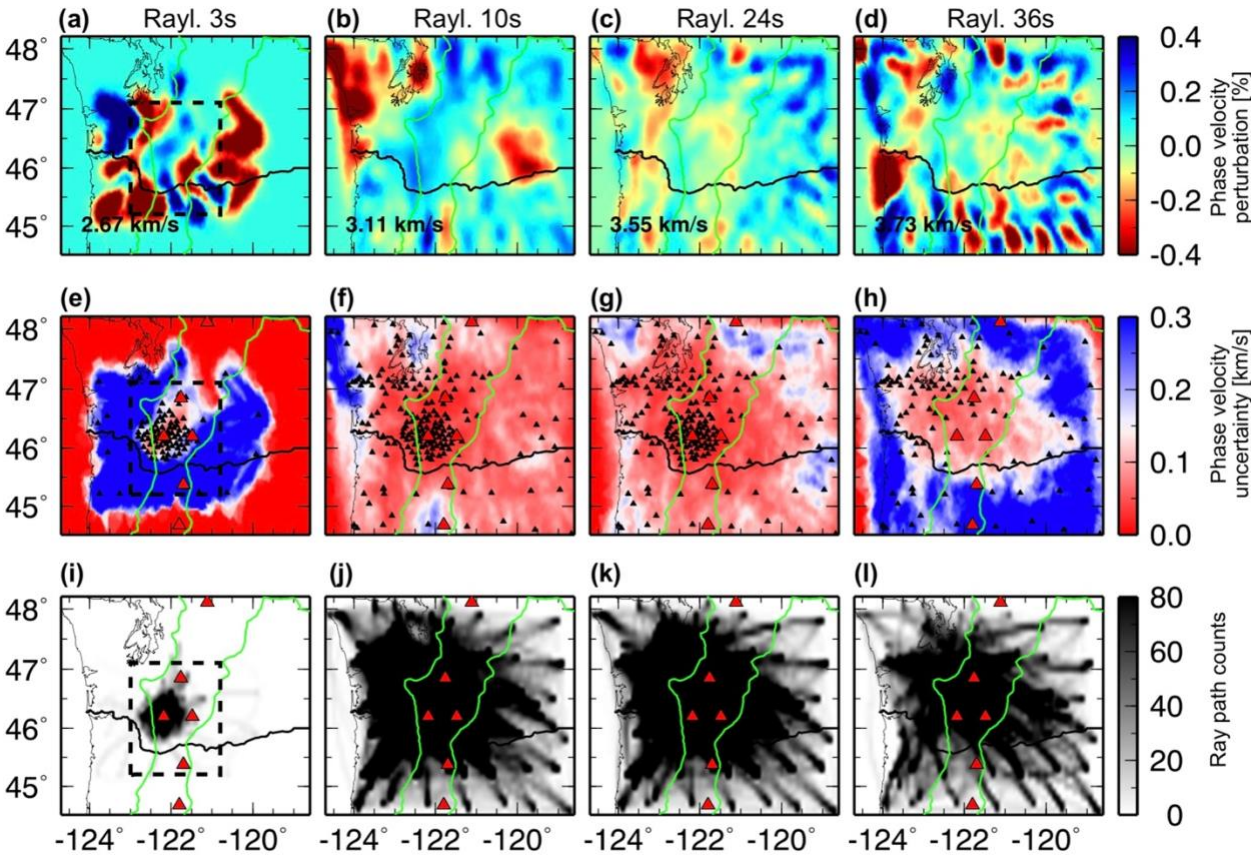

Figure S3. Rayleigh wave phase velocity maps, the associated uncertainty and ray path coverage at additional periods of 3s (a, e, i), 10 s (b, f, j), 24 s (c, g, k) and 36 s (d, h, l). The texts in the lower left of (a-d) indicate the regionally averaged phase velocity at each period. The black triangles in (e-h) show the station distribution at . The green lines denote the tectonic boundaries of the Cascades volcanic arc. The red triangles in (e-h) show the major Cascades arc volcanoes.

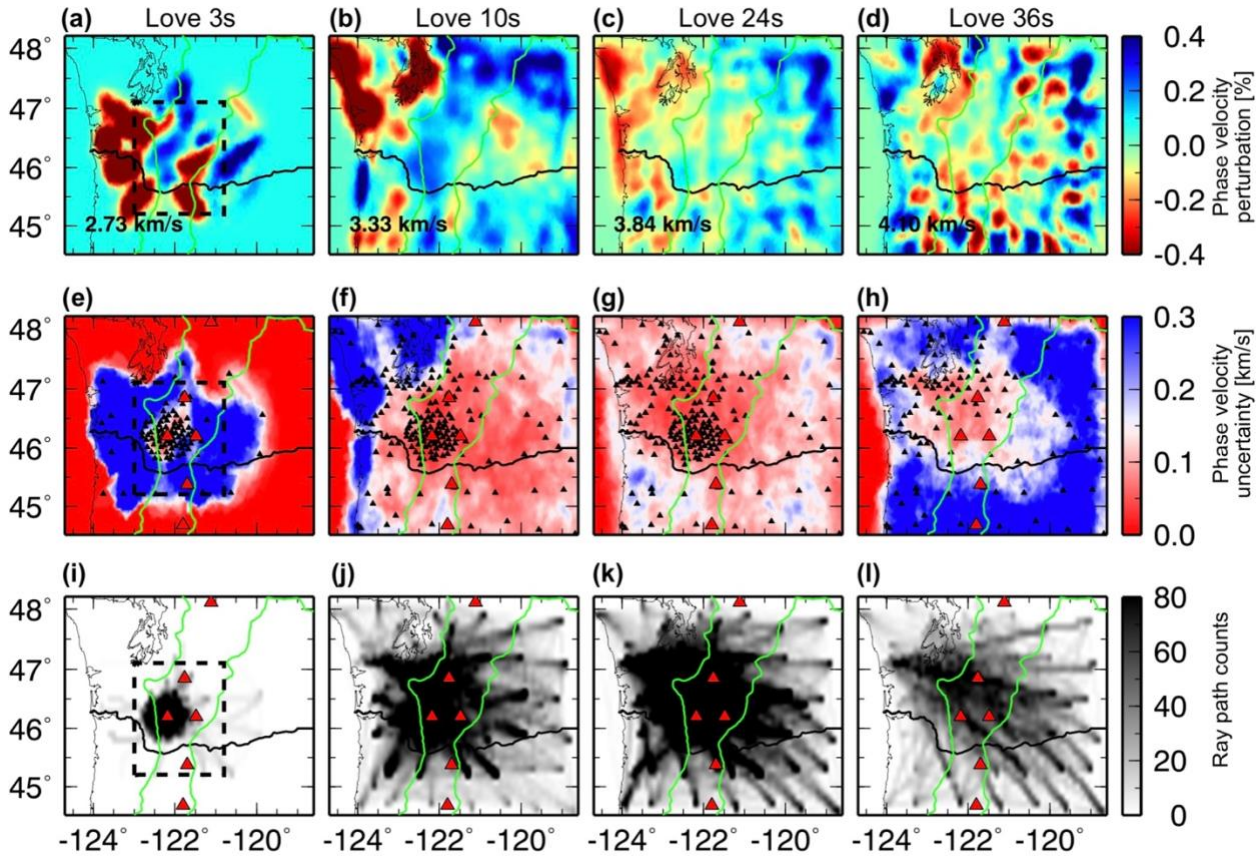

Figure S4. Same as Figure S3 but for Love wave.

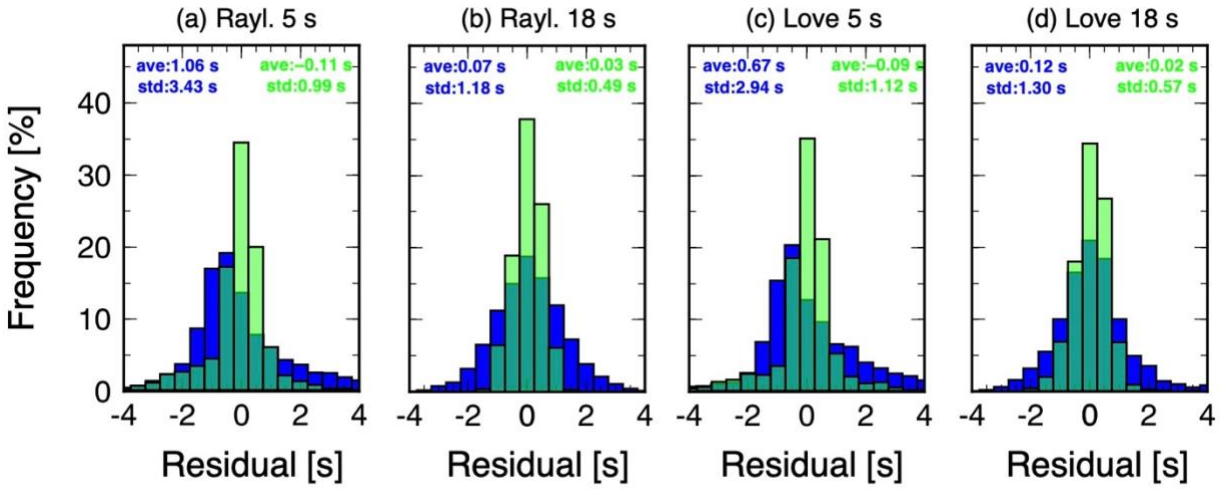

Figure S5. Traveltime residuals before (blue bars) and after (green bars) the tomography step at 5 and 18 s periods, for Rayleigh wave (a-b) and Love wave (c-d). The statistics of the distribution are shown by the color-coded texts on the top of each figure.

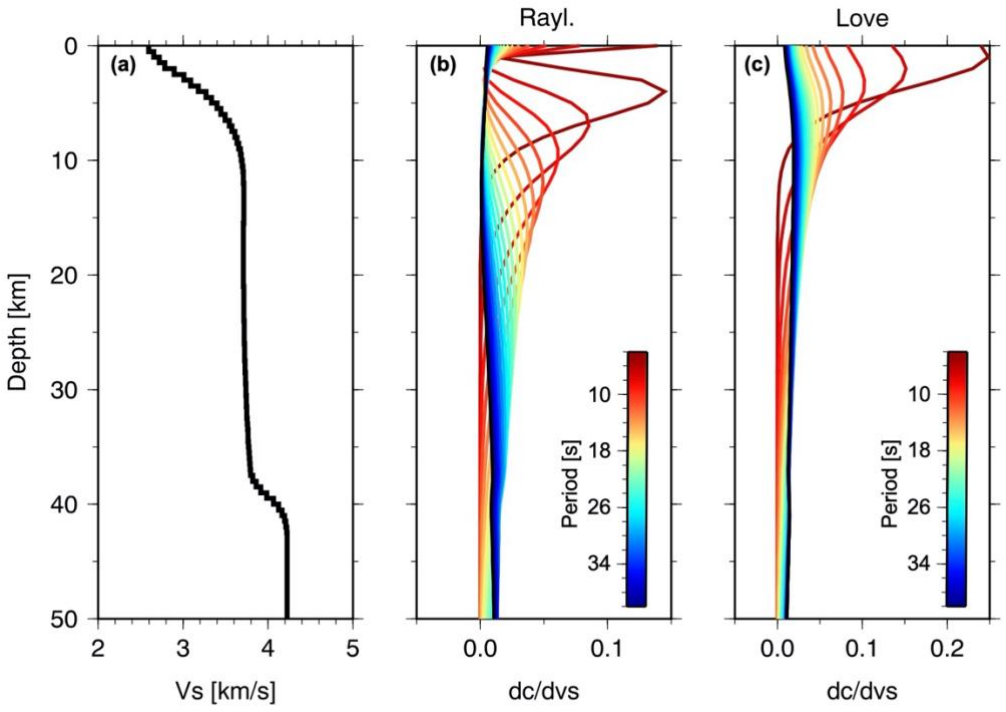

Figure S6. Sensitivity kernels of Rayleigh and Love waves as a function of depth for a series of period range. The velocity profile is from the inverted result right beneath the Mt. St. Helens.

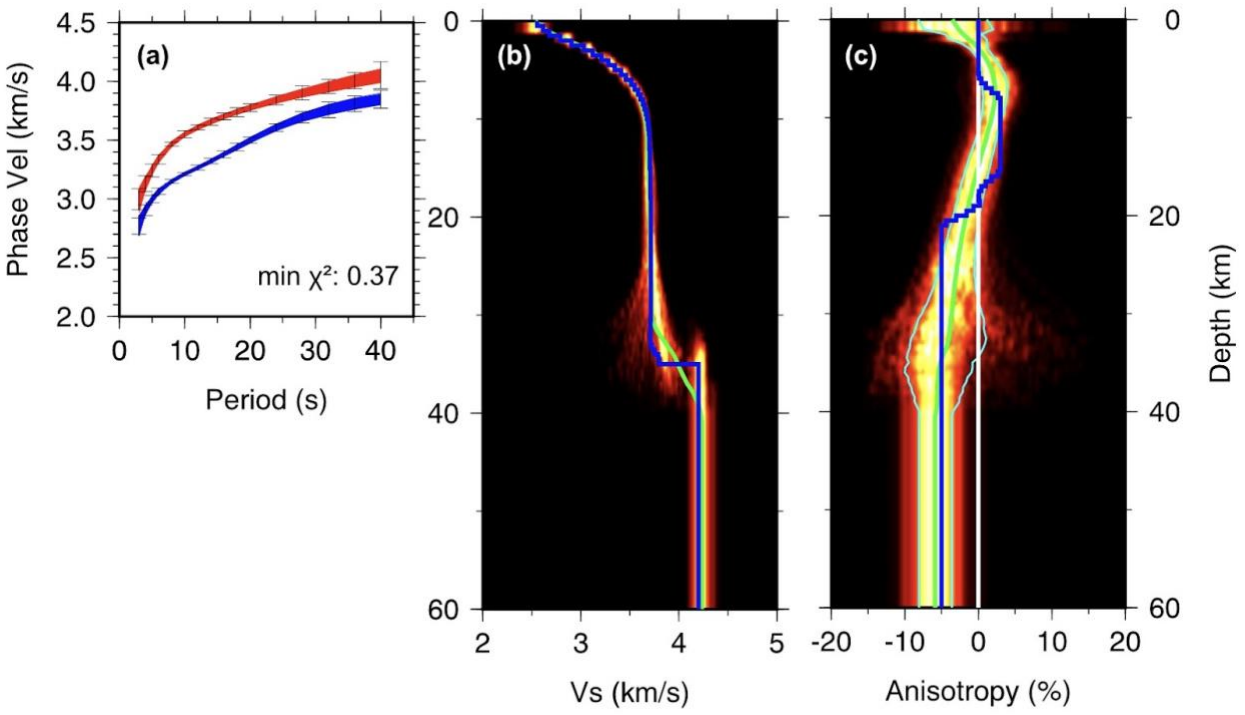

Figure S7. Synthetic test results using a realistic Vs profile beneath the MSH. (a) shows model fit of the inversion results. The error bars represent the observation and the blue and red lines show the predicted Rayleigh and Love wave dispersion from the ensemble of 2000 selected best models. (b) and (c) show the inverted isotropic and anisotropic profiles compared with the true model. The blue thick lines in (b) and (c) show the input models, while the green lines show the average of the ensemble of the McMC inversion. The cyan lines in (c) show the 1-sigma of the resulting anisotorpic profile.

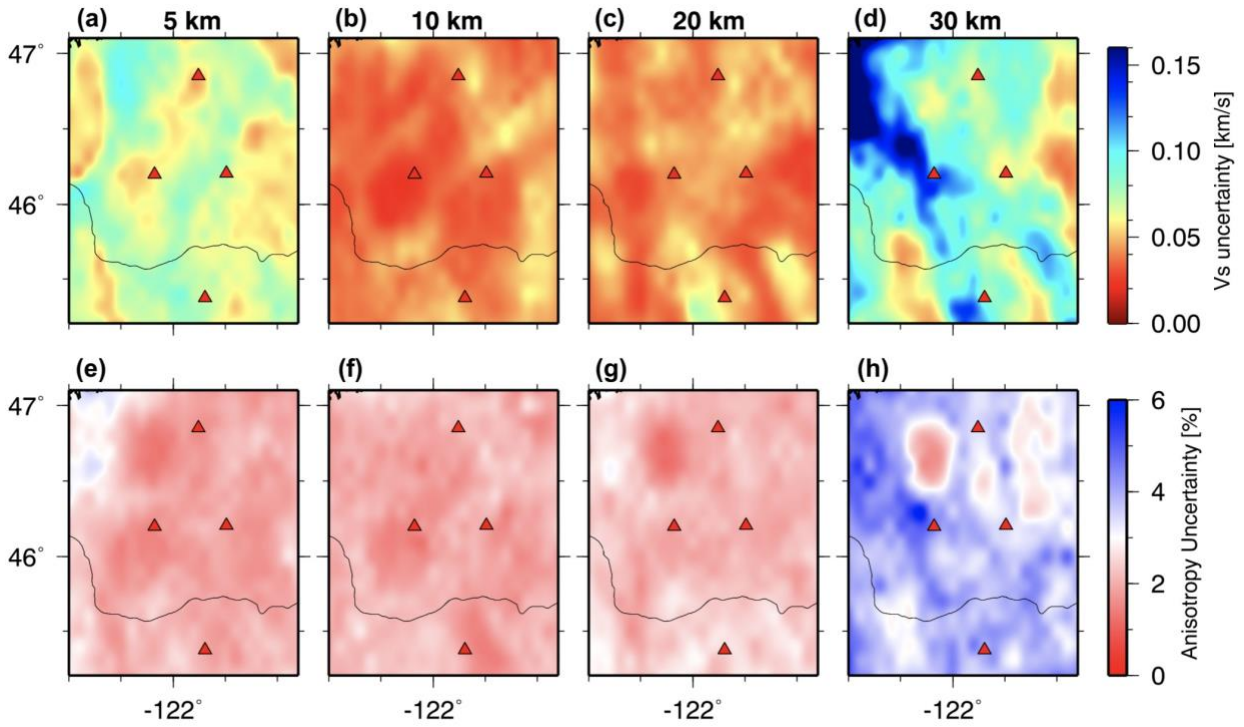

Figure S8. Uncertainties associated with the Vs (a-d) and anisotropy (e-h) component of the model in the region at 5, 10, 20 and 30 km, respectively.

References in supplements:

Brocher, T. M., Parsons, T., Tréhu, A. M., Snelson, C. M., & Fisher, M. A. (2003). Seismic evidence for widespread serpentinized forearc upper mantle along the Cascadia margin. *Geology*, 31(3), 267-270.

Buehler, J. S., & Shearer, P. M. (2017). Uppermost mantle seismic velocity structure beneath USArray. *Journal of Geophysical Research: Solid Earth*, 122(1), 436-448.

Hacker, B. R., Kelemen, P. B., & Behn, M. D. (2015). Continental lower crust. *Annual Review of Earth and Planetary Sciences*, 43(1), 167-205.

Julia, J., Ammon, C. J., Herrmann, R. B., & Correig, A. M. (2000). Joint inversion of receiver function and surface wave dispersion observations. *Geophysical Journal International*, 143(1), 99-112.

Kiser, E., Palomeras, I., Levander, A., Zelt, C., Harder, S., Schmandt, B., Hansen, S.M., Creager, K.C., & Ulberg, C. (2016). Magma reservoirs from the upper crust to the Moho inferred from high-resolution Vp and Vs models beneath Mount St. Helens, Washington State, USA. *Geology*, 44(6), 411-414.

Ma, X., & Lowry, A. R. (2017). USArray imaging of continental crust in the conterminous United States. *Tectonics*, 36(12), 2882-2902.

Mann, M. E., Abers, G. A., Crosbie, K., Creager, K., Ulberg, C., Moran, S., & Rondenay, S. (2019). Imaging subduction beneath Mount St. Helens: Implications for slab dehydration and magma transport. *Geophysical Research Letters*, 46(6), 3163-3171.

Miller, K. C., Keller, G. R., Gridley, J. M., Luetgert, J. H., Mooney, W. D., & Thybo, H. (1997). Crustal structure along the west flank of the Cascades, western Washington. *Journal of Geophysical Research: Solid Earth*, 102(B8), 17857-17873.

Parsons, T., Trehu, A. M., Luetgert, J. H., Miller, K., Kilbride, F., Wells, R. E., ... & Christensen, N. I. (1998). A new view into the Cascadia subduction zone and volcanic arc: Implications for earthquake hazards along the Washington margin. *Geology*, 26(3), 199-202.

Schmandt, B., Lin, F. C., & Karlstrom, K. E. (2015). Distinct crustal isostasy trends east and west of the Rocky Mountain Front. *Geophysical Research Letters*, 42(23), 10-290.

Shen, W., & Ritzwoller, M. H. (2016). Crustal and uppermost mantle structure beneath the United States. *Journal of Geophysical Research: Solid Earth*, 121(6), 4306-4342.

Tréhu, A. M., Asudeh, I., Brocher, T. M., Luetgert, J. H., Mooney, W. D., Nabelek, J. L., & Nakamura, Y. (1994). Crustal architecture of the Cascadia forearc. *Science*, 266(5183), 237-243.